

# Single-pixel tracking and imaging of a high-speed moving object

SHIJIAN LI,<sup>1,4</sup> YAN CAI,<sup>2,4</sup> YELIANG WANG,<sup>1</sup> XU-RI YAO,<sup>2,5</sup> AND QING ZHAO<sup>2,3,6</sup>

<sup>1</sup>*School of Integrated Circuits and Electronics, Beijing Institute of Technology, Beijing 100081, China*

<sup>2</sup>*Center for Quantum Technology Research and Key Laboratory of Advanced Optoelectronic Quantum Architecture and Measurements (MOE), School of Physics, Beijing Institute of Technology, Beijing 100081, China*

<sup>3</sup>*Beijing Academy of Quantum Information Sciences, Beijing 100193, China*

<sup>4</sup>*These two authors contribute equally to this work*

<sup>5</sup>[yaoxuri@bit.edu.cn](mailto:yaoxuri@bit.edu.cn)

<sup>6</sup>[qzhaoyuping@bit.edu.cn](mailto:qzhaoyuping@bit.edu.cn)

**Abstract:** Image-free tracking methods based on single-pixel detection have been able to track a moving object at a very high frame rate, but these tracking methods can not achieve simultaneous imaging of the object. Here we report a method for simultaneously tracking and imaging a high-speed moving object. Four binary Fourier patterns and two differential Hadamard patterns are used to modulate one frame of the object, then the modulated light signals are obtained by single-pixel detection. The trajectory and the image of the moving object can be gradually obtained along with the detection. The proposed method does not need any prior knowledge of the object and its motion. It has been verified by simulations and experiments which achieves a frame rate of 3332 Hz at a spatial resolution of  $128 \times 128$  pixels by using a 20000 Hz digital micromirror device. This proposed method can broaden the application of image-free tracking methods and realize the detection of spatial information of the moving object.

## 1. Introduction

Tracking and imaging a high-speed moving object have great application prospects in military, biomedical, computer vision, and other fields. The blurring caused by motion and the short exposure time caused by high frame rate shooting are the two main reasons that lead to the deterioration of imaging quality for a high-speed moving object. The high-speed camera [1] was invented to capture moving objects with a very high frame rate and relatively high signal-to-noise ratio, but the price is expensive and the data flux is very high. Various tracking and imaging methods for moving objects have been proposed based on spatial light modulators (SLM) and single-pixel detectors (SPD) with a wide spectral response [2–23].

Among these methods, the image-free method can achieve tracking a moving object at a very high frame rate. Zhang et al. proposed a real-time image-free tracking method based on the Fourier basis patterns and finally achieved a temporal resolution of 1666 frames per second (fps) with 10000 Hz digital micromirror device (DMD) [5]. Deng et al. extended the method to realize the three-dimensional trajectory tracking of a fast-moving object with 1666 fps [6]. Zha et al. proposed a fast moving object tracking method based on the geometric moment patterns and reached a frame rate of 7400 Hz [7]. Then Zha et al. continued proposing a complementary measurement scheme, which increased the frame rate of the method to 11.1 kHz [8]. However, the above methods cannot image the moving object when tracking the object at a high frame rate.

The single-pixel imaging (SPI) [24] based on SPD needs to use many modulation patterns to image the object, while the operating rate of the SLM used to modulate is limited, which causes the conflict between the sampling time and the reconstructed image quality. For a moving object, the sampling time allocated to a single moving frame is very short, and combining multiple

moving frames for calculation will lead to motion blur. To address this problem in SPI, a moving object can be imaged by estimating the moving speed of the object using an algorithm [10, 11], choosing the proper modulation patterns or increasing the speed of SLM to reduce the sampling time [12–17], and estimating motion information based on low-resolution images [18–20]. The methods by estimating motion information of the moving object are commonly used to image a moving object in recent years. Zhang et al. proposed a method to image a uniformly moving object by modifying the pattern and velocity parameters during reconstruction [10]. Jiao et al. proposed a method to estimate the motion parameters of the object under the assumption that the type of object motion is known [11]. In addition, many methods have been proposed to obtain the motion information of the object, such as calculating cross-correlation [18, 20] or low-order moments [19] of the images, using laterally shifting patterns [21], and projecting two-dimensional projective patterns [22]. Even so, the frame rate of these methods is far lower than that of the imaging-free tracking method. Inspired by the above methods, an idea of tracking and imaging moving an object naturally appears: we can first determine the object motion information through the image-free method, and then transform the spatial-coding patterns of the object using motion information; when the number of coding patterns is sufficient, the image of moving object can be reconstructed using the compressed sensing [25–27] algorithm. A similar idea is applied in the newest research. Guo et al. combined the geometric moment patterns and Hadamard patterns to achieve tracking and imaging of the moving object at a frame rate of 5.55 kHz [23].

In this paper, we design a new pattern sequence to achieve high frame rate trajectory detection and imaging of a high-speed moving object. Four binary Fourier patterns and two differential Hadamard patterns are used to modulating one frame of the object, then the modulated light signals are obtained by single-pixel detection. The displacement of the moving object for each moving frame can be determined by these six detection values. Based on the determined displacements and patterns, we can recalculate the reconstruction matrix and reconstruct the moving object image. Using this pattern sequence, The frame rate of tracking a moving object can catch up with that of the image-free method in Ref.[5]. The proposed method is verified by both simulations and experiments.

## 2. Method

In Fourier single-pixel imaging(FSPI) [28], the spatial information of the object is encoded by SLM using the Fourier basis patterns, and the series of modulated total light intensities are detected by a SPD. The required Fourier basis patterns are usually described by a pair of spatial frequencies and an initial phase. A Fourier basis pattern  $P(x, y)$  can be represented by its corresponding spatial frequency pair  $(f_x, f_y)$  and corresponding initial phase  $\phi_0$ :

$$P(x, y | f_x, f_y, \phi_0) = a_0 + b_0 \cos [2\pi (f_x x + f_y y) + \phi_0], \quad (1)$$

where  $a_0$  is the average intensity of the Fourier basis pattern,  $b_0$  is the contrast of the basis pattern, and  $(x, y)$  corresponds to the two-dimensional spatial coordinate of the basis pattern. The modulated total light intensity  $I$  can be obtained using the above Fourier basis patterns to modulate the illumination light or the detection area:

$$I = \sum_{x,y} O(x, y)P(x, y), \quad (2)$$

where  $O(x, y)$  is the object image. Based on the linear response of the single pixel detector to the light intensity within its effective detection range, the modulated light intensity can be replaced by the measured value of the SPD. The Fourier coefficients of the corresponding Fourier domain are obtained by these measured values. Four-step phase shift method and three-step phase shift method are two commonly used methods to obtain Fourier coefficients in FSPI [12]. The four-step phase shift method requires four Fourier basis patterns with the same spatial frequency but

different phases to obtain a Fourier coefficient. These four patterns are denoted as  $P(f_x, f_y, 0)$ ,  $P(f_x, f_y, \pi/2)$ ,  $P(f_x, f_y, \pi)$ , and  $P(f_x, f_y, 3\pi/2)$ , respectively. The corresponding single-pixel detection values are denoted as  $I_0$ ,  $I_{\pi/2}$ ,  $I_\pi$ , and  $I_{3\pi/2}$ , respectively. Then the corresponding Fourier coefficient is given by Eq.(3):

$$\tilde{O}(f_x, f_y) = (I_\pi - I_0) + j(I_{3\pi/2} - I_{\pi/2}), \quad (3)$$

it should be noted that the patterns  $P(f_x, f_y, 0)$  is the inverse of the pattern  $P(f_x, f_y, \pi)$ ,  $P(f_x, f_y, \pi/2)$  is the inverse of the pattern  $P(f_x, f_y, 3\pi/2)$ . Similarly, the three-step phase shift method requires three Fourier basis patterns with the same spatial frequency but different initial phases. These three patterns are respectively denoted as  $P(f_x, f_y, 0)$ ,  $P(f_x, f_y, 2\pi/3)$ , and  $P(f_x, f_y, 4\pi/3)$ . The corresponding single-pixel detection values are denoted as  $I_0$ ,  $I_{2\pi/3}$ , and  $I_{4\pi/3}$ , and the corresponding Fourier coefficient is given by Eq.(4):

$$\tilde{O}(f_x, f_y) = (2I_0 - I_{2\pi/3} - I_{4\pi/3}) + \sqrt{3}j(I_{2\pi/3} - I_{4\pi/3}), \quad (4)$$

the commonly used spatial light modulator in SPI is the DMD. These Fourier basis patterns are grayscale and cannot be directly loaded on the DMD. Binarization is usually required when these patterns are used for modulation. The grayscale patterns can be binarized using the upsampling scheme [12] and Floyd-Steinberg dithering method [29]. After binarization, the pattern  $P(f_x, f_y, 0)$  plus the pattern  $P(f_x, f_y, \pi)$  equals the all-one pattern; the pattern  $P(f_x, f_y, \pi/2)$  plus the pattern  $P(f_x, f_y, 3\pi/2)$  equals the all-one pattern, too.

In the Fourier transform, all points in the spatial domain will contribute to each coefficient in the Fourier domain, and the result is that the displacement change in the spatial domain will directly affect the Fourier coefficient. Based on the linear phase shift property of Fourier transform, Zhang et al. proposed a method to detect the object motion trajectory using two Fourier coefficients for each frame [5]. The specific principle is that the displacement  $(\Delta x, \Delta y)$  of the object image  $O(x, y)$  in the spatial domain will lead to the phase shift in the Fourier domain  $(-2\pi f_x \Delta x, -2\pi f_y \Delta y)$ , which can be expressed as:

$$O(x - \Delta x, y - \Delta y) = F^{-1} \left\{ \tilde{O}(f_x, f_y) \exp[-j2\pi(f_x \Delta x + f_y \Delta y)] \right\}, \quad (5)$$

where  $(f_x, f_y)$  is the spatial frequency coordinate in the Fourier domain,  $\tilde{O}(f_x, f_y)$  is the Fourier spectrum of the original image  $O(x, y)$ , and  $F^{-1}$  represents the inverse Fourier transform. The trajectory of the object can be calculated by measuring the phase shift term  $\varphi = -2\pi(f_x \Delta x + f_y \Delta y)$  of each frame. The displacement  $\Delta x$  and  $\Delta y$  is finally calculated by obtaining  $\tilde{O}(f_x, 0)$  and  $\tilde{O}(0, f_y)$  of each frame [5]:

$$\begin{aligned} \Delta x &= -\frac{1}{2\pi f_x} \cdot \arg \left\{ [\tilde{O}(f_x, 0) - \tilde{O}_{\text{bg}}(f_x, 0)] \right\}, \\ \Delta y &= -\frac{1}{2\pi f_y} \cdot \arg \left\{ [\tilde{O}(0, f_y) - \tilde{O}_{\text{bg}}(0, f_y)] \right\}, \end{aligned} \quad (6)$$

where  $\arg\{\}$  is the argument operation,  $\tilde{O}_{\text{bg}}(f_x, 0)$  and  $\tilde{O}_{\text{bg}}(0, f_y)$  represent the two Fourier coefficients obtained at the initial position before the object starts moving,  $\tilde{O}(0, f_y)$  and  $\tilde{O}(f_x, 0)$  represent the two Fourier coefficients obtained at the current moving frame. It has been verified that six binary Fourier basis patterns for each frame can realize real-time tracking of moving object trajectories by using the three-step phase shift method in Ref.[5].

As shown in Fig.1, the proposed pattern sequence consists of six patterns for each frame. Two differential Hadamard basis patterns that encoded the object spatial information are embedded in every four Fourier basis patterns for achieving the high rate of Ref.[5] and finally imaging the

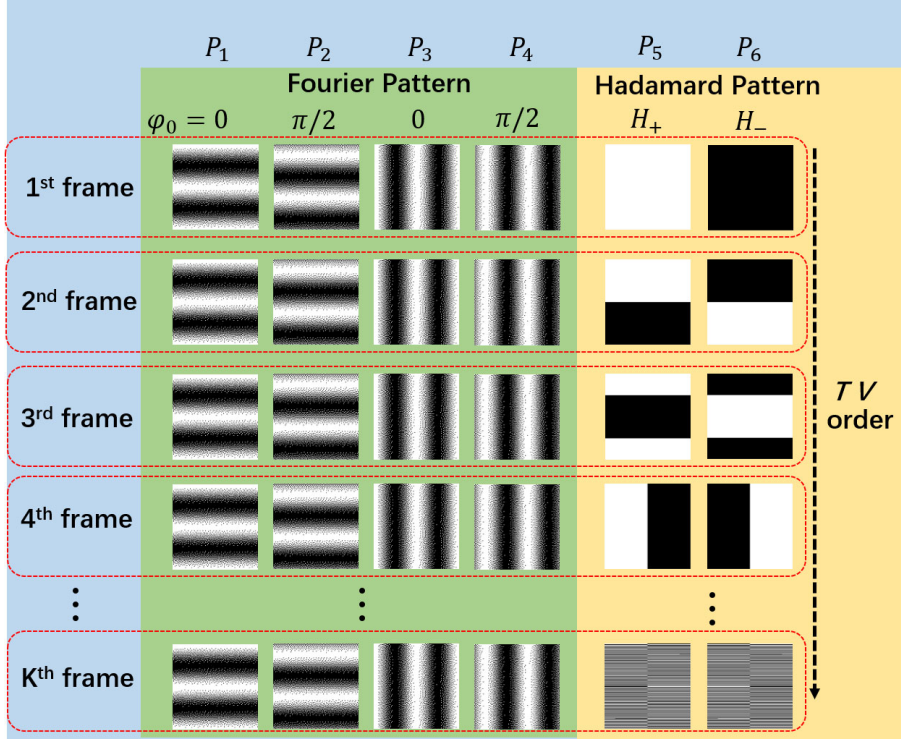


Fig. 1. Schematic diagram of pattern design. Each motion frame corresponds to six patterns, of which four are binary Fourier basis patterns and two are differential Hadamard basis patterns. The Fourier patterns of all frames are the same, and the corresponding phases are 0 and  $\pi/2$ , respectively. The Hadamard patterns corresponding to different motion frames are sorted according to the TV ordering method [30].

moving objects. The first four binary Fourier basis patterns of all motion frames are the same which is corresponding to the Fourier basis patterns of  $P(f_x, 0, 0)$ ,  $P(f_x, 0, \pi/2)$ ,  $P(0, f_y, 0)$ , and  $P(0, f_y, \pi/2)$ . The spatial frequency  $f_x$  and  $f_y$  in this work are both  $2/m$ , where  $m \times m$  is the spatial resolution of the image. The two differential Hadamard patterns  $H_+^k$  and  $H_-^k$  are calculated from the  $k^{\text{th}}$  Hadamard pattern  $H^k$ :

$$\begin{aligned} H_+^k &= (H^k + 1)/2, \\ H_-^k &= (1 - H^k)/2, \end{aligned} \quad (7)$$

$H_+^k$  plus  $H_-^k$  also equals the all-one pattern. The Hadamard patterns in each motion frame are different. Each Hadamard pattern is selected according to the total variation (TV) sorted method [30]. For six patterns of each frame, the corresponding single-pixel detection values are  $I_{x0}$ ,  $I_{x\pi/2}$ ,  $I_{y0}$ ,  $I_{y\pi/2}$ ,  $I_{H+}$ , and  $I_{H-}$ , respectively. Based on the four-step phase shift method, The two Fourier coefficients are calculated by:

$$\begin{aligned} \tilde{O}(f_x, 0) &= (I_{H+} + I_{H-} - 2I_{x0}) + j(I_{H+} + I_{H-} - 2I_{x\pi/2}), \\ \tilde{O}(0, f_y) &= (I_{H+} + I_{H-} - 2I_{y0}) + j(I_{H+} + I_{H-} - 2I_{y\pi/2}), \end{aligned} \quad (8)$$

and the Hadamard coefficient can be calculated by:

$$I_H = I_{H+} - I_{H-}, \quad (9)$$

The displacement of the object can be calculated by Eq.(6), and then the displacement of the

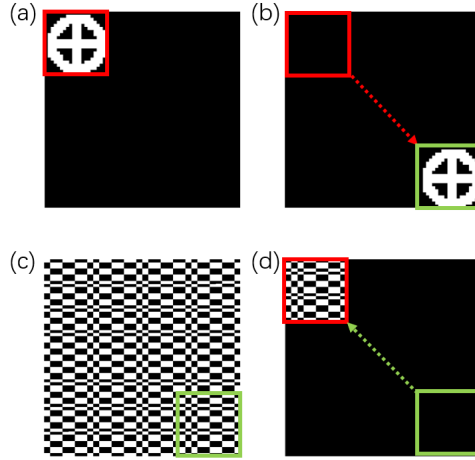


Fig. 2. Schematic diagram of modulating pattern transformation. (a) Initial position of the object; (b) Position of the object after movement; (c) Modulating pattern of the object after movement; (d) Transformed modulation pattern.

current frame can be determined. At the same time, four binary Fourier basis patterns, one Hadamard basis pattern, and the corresponding five single-pixel detection values are obtained for each frame which could be used for the final imaging procedure. The displacement of the object during the pattern modulation is equivalent to that the object is static and the pattern moves in the opposite direction to the object motion, then the object image can be reconstructed from the recorded single-pixel values and transformed patterns when transformed patterns are sufficient. The process of transforming pattern is shown in Fig.2. Total variation augmented lagrangian alternative direction algorithm (TVAL3) [31] is an efficient and widely used compressed sensing [25–27] algorithm. The TVAL3 solver can be adopted to reconstruct the object using the transformed patterns sequence and corresponding single-pixel detection values.

### 3. Results and discussion

#### 3.1. Simulations

In the simulation, An object with two trajectories is simulated for verifying the proposed method. The object image is shown in Fig.3(a), and the resolution is  $128 \times 128$  pixels. The total number of moving frames is 1666, and each frame corresponds to six patterns, meaning that a total of 9996 patterns are used in the simulation. As the two fastest image-free tracking methods, Zhang et al.'s method using binary Fourier patterns [5] and Zha et al.'s method using geometric moment patterns [7] are also simulated for comparison. The total number of patterns for Zhang et al.'s method [5] is also 9996, and 4998 patterns for Zha et al.'s method [7] correspond to 1666 moving frames. Hadamard patterns are selected to modulate and reconstruct the image of the moving object as the conventional single-pixel method, and 9996 differential Hadamard patterns are employed according to the TV order [30] for better quality. A Gaussian white noise with  $\sigma = 0.1$  is added to the measurement for simulating the real noisy experiments.

Mean Square Error (MSE) is introduced to evaluate the accuracy of the reconstructed trajectory. The MSE of the reconstructed trajectory coordinate  $Y$  and the original coordinate  $X$  is defined as

follows:

$$MSE(X, Y) = \frac{1}{n} \sum_{i=1}^n (X_i - Y_i)^2, \quad (10)$$

Where  $n$  is the total number of frames. The smaller the MSE, the closer the reconstructed trajectory is to the original trajectory. The peak signal-to-noise ratio (PSNR) and correlation coefficient (CC) are introduced to evaluate the quality of reconstructed images. The PSNR between the original image  $x$  and the reconstructed image  $y$  is defined as follows:

$$PSNR(x, y) = 10 \log \frac{peakval^2}{MSE(x, y)}, \quad (11)$$

Where  $MSE(x, y)$  is the mean square error between  $x$  and  $y$ .  $Peakval$  is the maximum value of the image data type. The higher the PSNR value, the higher the reconstruction quality. The CC between the original image  $x$  and the reconstructed image  $y$  is defined as follows:

$$CC(x, y) = \frac{cov(x, y)}{\sigma_x \sigma_y}, \quad (12)$$

Where  $cov(x, y)$  is the covariance of  $x$  and  $y$ ,  $\sigma_x$  is the standard deviation of  $x$ , and  $\sigma_y$  is the standard deviation of  $y$ . The value range of CC is  $[-1, 1]$ . The larger the CC value, the higher correlation between the two images.

The simulations with different noise distributions were repeated five times. Figure.3 shows the results of the corresponding method. The comparisons between the trajectories reconstructed by the three methods and the original trajectories are shown in Fig.3(b) and Fig.3(c). For trajectory (type-I) in Fig.3(b), the image reconstructed by conventional SPI and the proposed

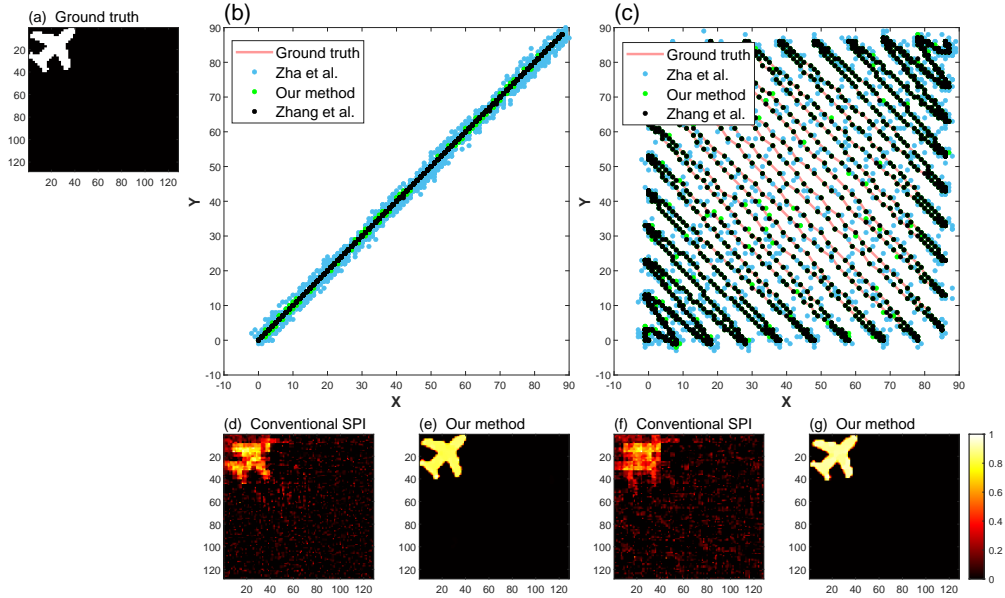


Fig. 3. Simulation results of one object with two trajectories. (a) Simulated object; (b) The type-I trajectories reconstructed by the three methods; (c) The type-II trajectories reconstructed by the three methods. (d) and (f) are the reconstructed images by the conventional SPI method. (e) and (g) are the reconstructed images by the proposed method.

Table 1. Comparisons of reconstructed trajectories and images using different methods

Trajectory	Method	Reconstructed trajectory		Reconstructed image	
		MSE	PSNR	CC	CC
Type-I	Conventional SPI	N/A	16.5285	0.7278	
	Zha et al.	4.0643	N/A	N/A	
	Zhang et al.	<b>0.0216</b>	N/A	N/A	
	Our method	0.3653	<b>25.5548</b>	<b>0.9792</b>	
Type-II	Conventional SPI	N/A	16.1369	0.7000	
	Zha et al.	4.1906	N/A	N/A	
	Zhang et al.	<b>0.0212</b>	N/A	N/A	
	Our method	0.2384	<b>26.3454</b>	<b>0.9834</b>	

method are shown in Fig.3(d) and Fig.3(e), respectively. For trajectory (type-II) in Fig.3(c), the images reconstructed by conventional SPI and the proposed method are shown in Fig.3(f) and Fig.3(g). Table.1 shows the mean MSEs,PSNRs, and CCs of these methods.It can be seen from the above results that both Zhang et al.'s method [5] and the proposed method can reconstruct the trajectories of the moving object well in the presence of noise, among which the Zhang et al.'s method [5] is the best, followed by the proposed method, and the Zha et al.'s method [7] has a large deviation in the reconstructed trajectories, indicating that the geometric moment patterns are more sensitive to noise. The reconstructed images of the conventional SPI method are blurred and degraded because of the motion of the object in the measurement process, while the proposed method can reconstruct the images of the moving object well.

The influence of the number of moving frames on the imaging quality should be also considered by reconstruct the image using sequentially reducing number of frames. The reconstructed images of moving along the Type-II trajectory were studied in this simulation. Twenty groups of data were selected, including 5%, 10%, 15%,..., 95%, and 100% of the total 1666 frames, respectively, to calculate the reconstructed images. The corresponding PSNRs and CCs are shown in Fig.4(a). Figure4(b-e) shows the reconstructed images with the corresponding frame

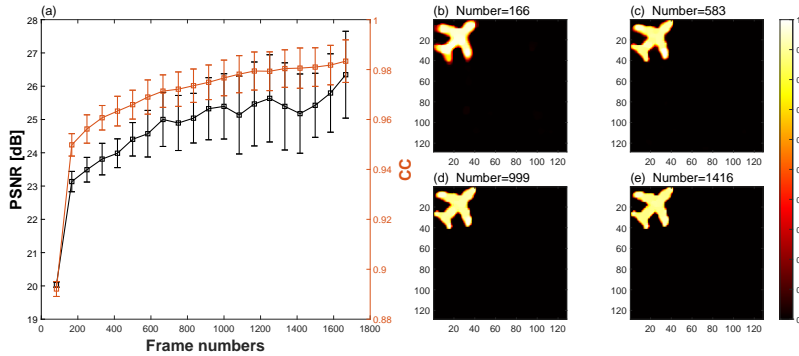


Fig. 4. The influence of the number of moving frames measured by the proposed method on the imaging quality. (a) The PSNRs and CCs of the reconstructed images using different numbers of frames ; (b-e) the reconstructed images using 166, 583, 999, and 1416 frames, respectively.

numbers 166, 583, 999, and 1416. The results indicate that considering the influence of noise when the number of sampling frames is more than a certain frame number (e.g., 333 frames), the moving object image with good quality can be reconstructed.

### 3.2. Experiments

The proposed method is verified through experiments. The experimental system device consists of a light-emitting diode (LED) source with a maximum power of 5 W, a linear motorized stage(GCD-302003M, Daheng Optics), a digital micromirror device (DMD, Texas Instruments DLP7000), a photomultiplier tube(PMT, H10682-01, Hamamatsu Photonics), and a data acquisition board, as show in Fig.5. The modulation patterns are preloaded into the DMD in advance for modulation.

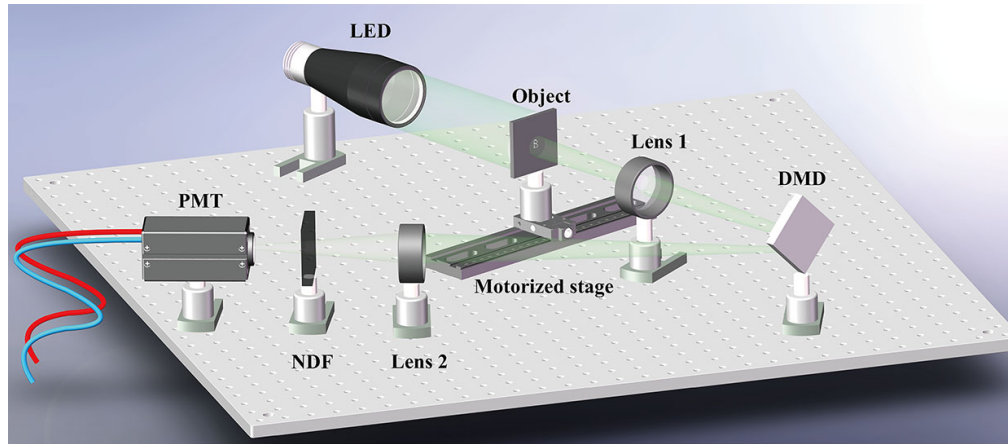


Fig. 5. Experimental setup. A motorized stage moves the object in one directions. The transmitted object is imaged on the digital micromirror device (DMD) after being illuminated by the light-emitting diode (LED) source. After being modulated by the DMD, the modulated light is collected into the photomultiplier tube (PMT) and converted into the measurement values through the data acquisition board. NDF: neutral density filter.

The transmitted object is imaged on the DMD after being illuminated by the light source. After being modulated by the DMD, the modulated light is collected into the PMT and converted into the measurement values through the data acquisition board. In this section, a total of two groups of experiments are set. In the first group of experiments, a linear motorized stage with a maximum speed of 9.87 mm/s was used to experiment of moving objects at a constant speed. In the second group of experiments, the acceleration movement experiment was realized with a mounting platform that slid along a rail. The mounting platform was connected to a suspended weight using a pulley. The DMD operated at a high refresh rate of 20000 Hz. The pixel size of the modulation patterns located on the DMD was  $256 \times 256$  pixels, and every  $2 \times 2$  pixels were merged into one super pixel, which meant that the image size of the moving object was  $128 \times 128$  pixels. The Fourier basis patterns used in the method were binarized by the Floyd-Steinberg dithering algorithm [29] with an upsampling rate of one. In each group of experiments, a total of 9,996 patterns were used corresponding to a frame numbers of 1666, and the total measurement time was 0.4998 s for modulating rate of 20000 Hz.

#### 3.2.1. Moving objects at a constant speed

In the experiment in this section, the moving objects were a transmitted object "B" with a size of  $2.5 \text{ mm} \times 3.2 \text{ mm}$  and a transmitted object "star" with a size of  $10 \text{ mm} \times 10 \text{ mm}$ , and the spatial

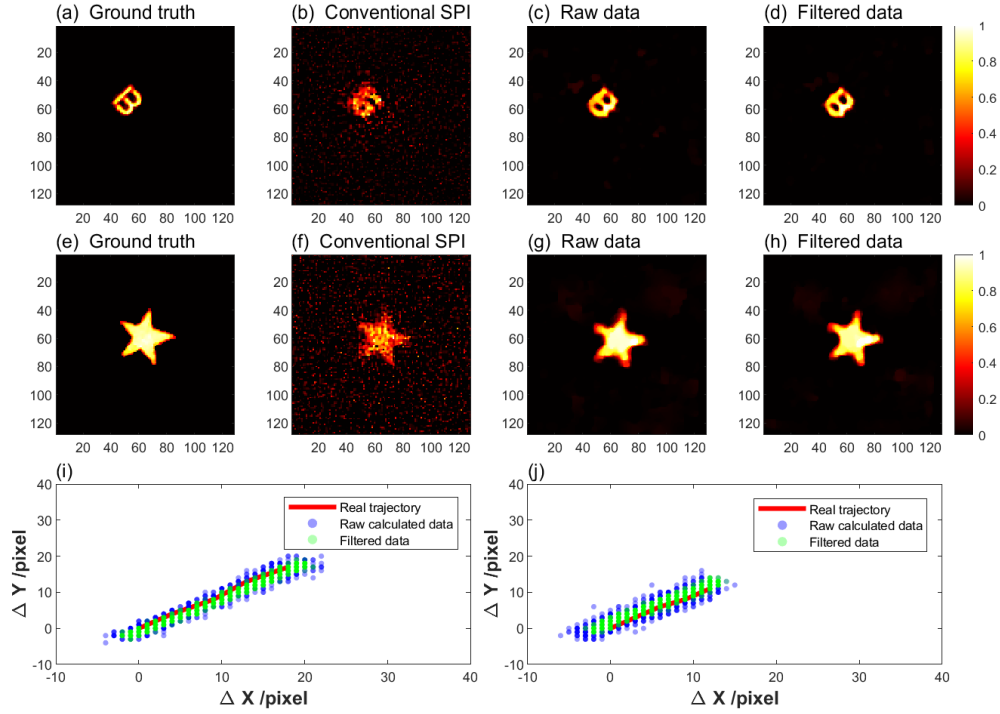


Fig. 6. The imaging and tracking results of two moving objects. (a) and (b) are the Ground truth images.(b) and (d) are the reconstructed moving objects by conventional SPI. (c) and (g) are the reconstructed moving objects by the proposed method using raw data. (d) and (h) are the reconstructed moving objects by the proposed method using filtered data. (i) and (j) are the comparison of the real trajectory and calculated trajectory.

resolution of both objects' images was  $128 \times 128$  pixels. Both moving objects move linearly along the diagonal of the image at the maximum speed of 9.87 mm/s of the linear motorized stage. The ground truth images were obtained by imaging the static object using the conventional SPI method, as shown in Fig.6(a) and Fig.6(e). To obtain a clear static image, the DMD was operated at a modulating rate of 1000 Hz. A total of 9996 differential Hadamard patterns were also used corresponding to a sample ratio of 30.51%. The reconstructed images for moving objects using the conventional SPI method are shown in Fig.6(b) and Fig.6(f), which get blurred because of motion. Two images of moving objects with good quality were calculated by the proposed

Table 2. The quality of reconstructed trajectories and images without/with a filter

Object	Data	Reconstructed trajectory		Reconstructed image
		MSE	PSNR	CC
"B"	Raw data	5.6002	29.4822	0.9303
	Filtered data	<b>4.1789</b>	<b>29.6327</b>	<b>0.9432</b>
"Star"	Raw data	5.3944	28.2537	0.7837
	Filtered data	<b>2.9082</b>	<b>29.5700</b>	<b>0.8165</b>

method, as shown in Fig.6(c) and Fig.6(g). Figure.6(i) and Figure.6(j) are the comparisons between the real trajectory and the calculated trajectory by the proposed method. The real trajectory of the object was determined by imaging the static object along the displacement axis of the motorized stage. Five static object images reconstructed by the conventional SPI method were combined to obtain the real trajectory. The quality of reconstructed trajectories and images improves by adopting a five-order mean filter to the calculated Fourier coefficients, as shown in Tab.2. And the reconstructed images using filtered data are shown in Fig.6(d) and Fig.6(h).

### 3.2.2. The acceleration movement experiment

The moving object "star" was selected to perform an acceleration movement experiment. The object was placed on a mounting platform that slid along a rail and connected by a horizontal thin rope to a fixed pulley and a weight of appropriate size. By adjusting the weight, the transmission object could be accelerated along the linear guide rail from a standstill. When the object started to move, the detection module began counting until all the patterns of 9996 frames were loaded. The average speed of the moving object was 55.7 mm/s. The reconstructed trajectory using Zhang et al.'s method [5] is also plotted in Fig.7(a) for comparison. It could be seen from Fig.7(a) that Zhang et al.'s method [5] and the proposed method reconstruct the same trajectories of the moving object in the experiment, among which the trajectory using filtered data had a smaller deviation. The trajectory of the object in the X and Y direction indicates the characteristics of the object's accelerated motion, as shown in Fig.7(b). The reconstructed images using the conventional SPI method is shown in Fig.7(c), which get more blurred than the above uniform motion experiment. Figure.6(d) shows the reconstructed image by the proposed method using raw data. Figure.6(e) is the reconstructed image by proposed method using filtered data.

The influence of the number of moving frames measured on the imaging quality was studied in this experiment. Twenty groups of measured data were selected, including 5%, 10%, 15%,..., 95%, and 100% of the total 1666 frames, respectively, to calculate the reconstructed images. The corresponding PSNRs and CCs are shown in Fig.8(a). The reconstructed images with the

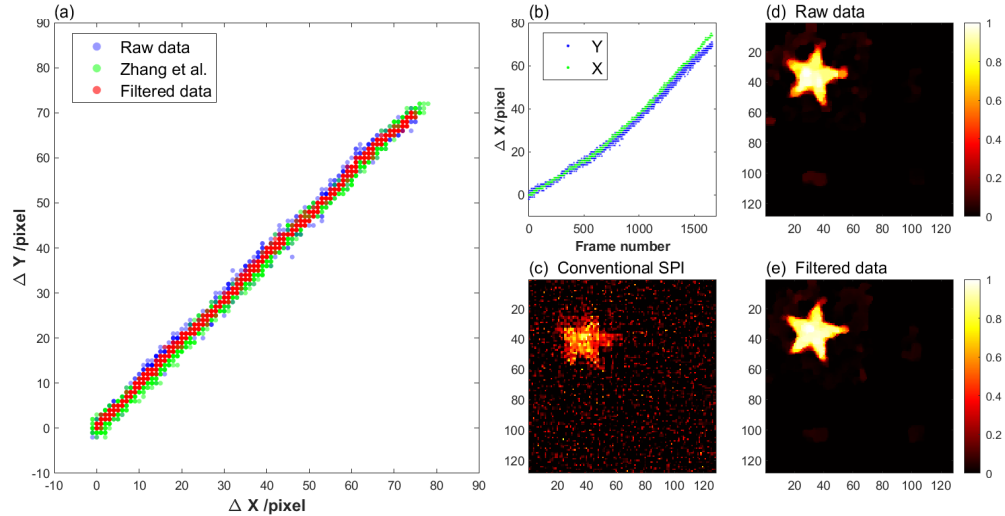


Fig. 7. Experimental results of an accelerating moving object. (a) The comparison of calculated trajectory; (b) The trajectory of the object in the X and Y direction.(c)The reconstructed moving objects by conventional SPI.(d)The reconstructed moving objects by the proposed method using raw data.(e)The reconstructed moving objects by the proposed method using filtered data.

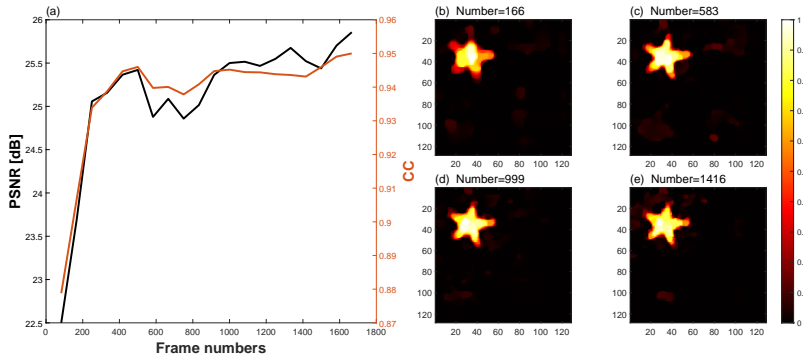


Fig. 8. Experiment on the contribution of the number of measured moving frames to reconstructed imaging quality. (a) The PSNRs and CCs of the reconstructed images using different numbers of frames; (b-e) the reconstructed images using 166, 583, 999, and 1416 frames, respectively.

corresponding frame numbers 166, 583, 999, and 1416 are shown in Fig.8(b-e). The above experimental results are similar to that in the simulation.

### 3.3. Discussion

The key of the proposed method is to use the object motion information determined by the image-free tracking method. The higher the frame rate and the more accurate the calculated trajectory, the more accurate the reconstructed image of the moving object. In the experiment, six modulation patterns were used for each motion frame. Combining a DMD with the refresh rate of 20000 Hz, we achieved tracking at a frame rate of 3332 Hz and finally imaged the moving object. The higher frame rate can be achieved by using an SLM with a higher refresh rate. Although a higher tracking frame rate can be achieved based on geometric moments patterns, the simulation indicates that the binary geometric moment patterns [7] require a higher upsampling rate when binarization and lack of differential measurement, which will lead to loss of spatial resolution and worse robustness to noise than the Fourier patterns. Four-step phase shift method has usually better noise resistance than the three-step phase shift method to obtain a Fourier coefficient [32], but the variance of the trajectories reconstructed by our method is slightly larger than Zhang et al.'s method [5]. The main reason is that six measured values are used to calculate the Fourier coefficients rather than the eight values required by the four-step phase shift method. The median filter is used to reduce the fluctuation of the reconstructed trajectory and obtain better images. The simulated and experimental results indicate that with the increase in the number of measurement frames, the quality of the reconstructed image will increase sharply and then tend to be stable. We also acknowledge that the proposed method has several limitations. Firstly, it can only track and image a transnational object with a simple background in the field of view. Secondly, the image cannot be reconstructed in real-time due to the iterative algorithm. Thirdly, the method can not reconstruct the image if the object moves too fast to obtain enough useful measurements. Solving the above limitations will be our future work.

## 4. Conclusion

A single-pixel detection method for object tracking and imaging is proposed in this paper. The displacement of a moving object for each moving frame can be determined by four Fourier patterns plus two differential Hadamard patterns. Based on the determined displacements and patterns, we can recalculate the reconstruction matrix and reconstruct the image of the moving

object. This method does not need any prior knowledge of the object and its motion. It has been verified by simulations and experiments which achieves a frame rate of 3332 Hz at a spatial resolution of  $128 \times 128$  pixels by using a 20000 Hz DMD. Future works can focus on extending to the imaging of rotating objects and accelerating the reconstruction process to finally realizing real-time imaging.

#### Funding.

**Disclosures.** The authors declare no conflicts of interest.

**Data availability.** Data underlying the results presented in this paper are not publicly available at this time but may be obtained from the authors upon reasonable request.

#### References

1. Y. Kondo, K. Takubo, H. Tominaga, R. Hirose, N. Tokuoka, Y. Kawaguchi, Y. Takaie, A. Ozaki, S. Nakaya, F. Yano, and T. Daigen, "Development of "hypervision hpv-x" high-speed video camera," *Shimadzu Rev.* **69**, 285–291 (2012).
2. H. Jiang, S. Zhu, H. Zhao, B. Xu, and X. Li, "Adaptive regional single-pixel imaging based on the Fourier slice theorem," *Opt. Express* **25**, 15118–15130 (2017).
3. H. Jiang, H. Liu, X. Li, and H. Zhao, "Efficient regional single-pixel imaging for multiple objects based on projective reconstruction theorem," *Opt. Lasers Eng.* **110**, 33–40 (2018).
4. D. Shi, K. Yin, J. Huang, K. Yuan, W. Zhu, C. Xie, D. Liu, and Y. Wang, "Fast tracking of moving objects using single-pixel imaging," *Opt. Commun.* **440**, 155–162 (2019).
5. Z. Zhang, J. Ye, Q. Deng, and J. Zhong, "Image-free real-time detection and tracking of fast moving object using a single-pixel detector," *Opt. Express* **27**, 35394–35401 (2019).
6. Q. Deng, Z. Zhang, and J. Zhong, "Image-free real-time 3-D tracking of a fast-moving object using dual-pixel detection," *Opt. Lett.* **45**, 4734–4737 (2020).
7. L. Zha, D. Shi, J. Huang, K. Yuan, W. Meng, W. Yang, R. Jiang, Y. Chen, and Y. Wang, "Single-pixel tracking of fast-moving object using geometric moment detection," *Opt. Express* **29**, 30327–30336 (2021).
8. L. Zha, W. Meng, D. Shi, J. Huang, K. Yuan, W. Yang, Y. Chen, and Y. Wang, "Complementary moment detection for tracking a fast-moving object using dual single-pixel detectors," *Opt. Lett.* **47**, 870–873 (2022).
9. Z.-H. Yang, X. Chen, Z.-H. Zhao, M.-Y. Song, Y. Liu, Z.-D. Zhao, H.-D. Lei, Y.-J. Yu, and L.-A. Wu, "Image-free real-time target tracking by single-pixel detection," *Opt. Express* **30**, 864–873 (2022).
10. C. Zhang, W. Gong, and S. Han, "Improving imaging resolution of shaking targets by Fourier-transform ghost diffraction," *Appl. Phys. Lett.* **102**, 021111 (2013).
11. S. Jiao, M. Sun, Y. Gao, T. Lei, Z. Xie, and X. Yuan, "Motion estimation and quality enhancement for a single image in dynamic single-pixel imaging," *Opt. Express* **27**, 12841–12854 (2019).
12. Z. Zhang, X. Wang, G. Zheng, and J. Zhong, "Fast Fourier single-pixel imaging via binary illumination," *Sci. Reports* **7**, 1–9 (2017).
13. Z.-H. Xu, W. Chen, J. Penuelas, M. Padgett, and M.-J. Sun, "1000-fps computational ghost imaging using LED-based structured illumination," *Opt. Express* **26**, 2427–2434 (2018).
14. W. Jiang, X. Li, X. Peng, and B. Sun, "Imaging high-speed moving targets with a single-pixel detector," *Opt. Express* **28**, 7889–7897 (2020).
15. E. Hahamovich, S. Monin, Y. Hazan, and A. Rosenthal, "Single pixel imaging at megahertz switching rates via cyclic Hadamard masks," *Nat. Commun.* **12**, 1–6 (2021).
16. W. Jiang, J. Jiao, Y. Guo, B. Chen, Y. Wang, and B. Sun, "Single-pixel camera based on a spinning mask," *Opt. Lett.* **46**, 4859–4862 (2021).
17. S. Monin, E. Hahamovich, and A. Rosenthal, "Single-pixel imaging of dynamic objects using multi-frame motion estimation," *Sci. reports* **11**, 1–11 (2021).
18. S. Sun, J.-H. Gu, H.-Z. Lin, L. Jiang, and W.-T. Liu, "Gradual ghost imaging of moving objects by tracking based on cross correlation," *Opt. Lett.* **44**, 5594–5597 (2019).
19. D. Yang, C. Chang, G. Wu, B. Luo, and L. Yin, "Compressive ghost imaging of the moving object using the low-order moments," *Appl. Sci.* **10**, 7941 (2020).
20. J. Wu, L. Hu, and J. Wang, "Fast tracking and imaging of a moving object with single-pixel imaging," *Opt. Express* **29**, 42589–42598 (2021).
21. S. Sun, H.-K. Hu, Y.-K. Xu, Y.-G. Li, H.-Z. Lin, and W.-T. Liu, "Simultaneously tracking and imaging a moving object under photon crisis," *Phys. Rev. Appl.* **17**, 024050 (2022).
22. W. Yang, D. Shi, K. Han, Z. Guo, Y. Chen, J. Huang, H. Ling, and Y. Wang, "Anti-motion blur single-pixel imaging with calibrated radon spectrum," *Opt. Lett.* **47**, 3123–3126 (2022).
23. Z. Guo, W. Meng, D. Shi, L. Zha, W. Yang, J. Huang, Y. Chen, and Y. Wang, "Fast localization and single-pixel imaging of the moving object using time-division multiplexing," *arXiv:2208.07371* (2022).
24. M. P. Edgar, G. M. Gibson, and M. J. Padgett, "Principles and prospects for single-pixel imaging," *Nat. photonics* **13**, 13–20 (2019).

25. D. L. Donoho, "Compressed sensing," *IEEE Transactions on information theory* **52**, 1289–1306 (2006).
26. E. J. Candès and M. B. Wakin, "An introduction to compressive sampling," *IEEE Signal Process. Mag.* **25**, 21–30 (2008).
27. M. F. Duarte, M. A. Davenport, D. Takhar, J. N. Laska, T. Sun, K. F. Kelly, and R. G. Baraniuk, "Single-pixel imaging via compressive sampling," *IEEE Signal Process. Mag.* **25**, 83–91 (2008).
28. Z. Zhang, X. Ma, and J. Zhong, "Single-pixel imaging by means of Fourier spectrum acquisition," *Nat. Commun.* **6**, 1–6 (2015).
29. R. W. Floyd and L. Steinberg, "An adaptive algorithm for spatial gray-scale," *Proc. Soc. Inf. Disp.* **17**, 75–77 (1976).
30. X. Yu, R. I. Stantchev, F. Yang, and E. Pickwell-MacPherson, "Super sub-nyquist single-pixel imaging by total variation ascending ordering of the hadamard basis," *Sci. Reports* **10**, 1–11 (2020).
31. C. Li, W. Yin, H. Jiang, and Y. Zhang, "An efficient augmented Lagrangian method with applications to total variation minimization," *Comput. Optim. Appl.* **56**, 507–530 (2013).
32. Z. Zhang, X. Wang, G. Zheng, and J. Zhong, "Hadamard single-pixel imaging versus Fourier single-pixel imaging," *Opt. Express* **25**, 19619–19639 (2017).